Heliyon 10 (2024) e34436

Contents lists available at ScienceDirect

Heliyon

journal homepage: www.cell.com/heliyon

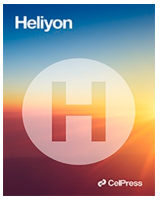

Research article

Fabrication electro-spun Poly(vinyl alcohol)-Melamine nonwoven membrane composite separator for high-power lithium-ion batteries

Xiao-Wei Wu [a,b], Manojkumar Seenivasan [a], Chelladurai Karuppiah [a,**], Bo-Rong Zhang [a,b], Jeng-Ywan Shih [a,b], Ying-Jeng James Li [a,b], Tai-Feng Hung [a], Wen-Chen Chien [a,b], Sayee Kannan Ramaraj [c], Rajan Jose [d], Chun-Chen Yang [a,b,e,*]

[a] *Battery Research Center of Green Energy, Ming Chi University of Technology, New Taipei City, 24301, Taiwan, R.O.C*
[b] *Department of Chemical Engineering, Ming Chi University of Technology, New Taipei City 243, Taiwan, R.O.C*
[c] *PG and Research Department of Chemistry, Thiagarajar College, Madurai, Tamil Nadu, India*
[d] *Nanostructured Renewable Energy Materials Laboratory, Faculty of Industrial Sciences and Technology, University Malaysia Pahang, 26300 Kuantan, Malaysia*
[e] *Department of Chemical and Materials Engineering & Center for Sustainability and Energy Technologies, Chang Gung University, Taoyuan City 333, Taiwan*

A R T I C L E I N F O

Keywords:
Electrospinning
Nonwoven
Composite separators
PVA polymers
Surface modification
Rechargeable Li-ion batteries

A B S T R A C T

Current commercial separators used in lithium-ion batteries have inherent flaws, especially poor thermal stability, which pose substantial safety risks. This study introduces a high-safety composite membrane made from electrospun poly(vinyl alcohol)-melamine (PVAM) and polyvinylidene fluoride (PVDF) polymer solutions via a dip coating method, designed for high-voltage battery systems. The poly(vinyl alcohol) and melamine components enhance battery safety, while the PVDF coating improves lithium-ion conductivity. The dip-coated PVDF/Esp-PVAM composite separators were evaluated for electrolyte uptake, contact angle, thermal stability, porosity, electrochemical stability and ionic conductivity. Notably, our Dip 1 % PVDF@Esp-PVAM composite separator exhibited excellent wettability and a lithium-ion conductivity of approximately 7.75×10^{-4} S cm^{-1} at room temperature. These separators outperformed conventional PE separators in half-cells with Ni-rich NCM811 cathodes, showing exceptional cycling stability with 93.4 % capacity retention after 100 cycles at 1C/1C, as compared to 84.8 % for PE separators. Our Dip 1 % PVDF@Esp-PVAM composite separator demonstrates significant potential for enhancing the long-term durability and high-rate performance of lithium-ion batteries, making it a promising option for long-term energy storage applications.

1. Introduction

In recent years, there has been a global surge in environmental awareness, prompting countries like the United Kingdom, China, France, and Germany to enact policies that phase out fuel-powered vehicles in favor of electric cars [1,2]. The future trajectory of the

* Corresponding author.Battery Research Center of Green Energy, Ming Chi University of Technology, New Taipei City, 24301, Taiwan, R.O.C.
** Corresponding author.
E-mail addresses: kcdurai.rmd@gmail.com (C. Karuppiah), ccyang@mail.mcut.edu.tw (C.-C. Yang).

https://doi.org/10.1016/j.heliyon.2024.e34436
Received 1 April 2024; Received in revised form 24 June 2024; Accepted 9 July 2024

automotive industry hinges on the rise of electric vehicles (EVs), with their success critically dependent on the pivotal role of lithium-ion batteries (LIBs) [3]. Owing to their high energy density, high operating voltage, and extended cycle life, lithium-ion batteries (LIBs) are poised to be pivotal in future energy storage solutions. Separators in LIBs play a crucial role by dividing the cathode and anode, enabling rapid ion transport, and enhancing performance while preventing overcharging, thermal runaway, and electronic short circuits [4]. The Li ions in liquid electrolytes can freely transport across separator membranes because of their microporous nature as they are also chemically inert during electrochemical reactions and therefore doesn't participate in the reaction while protecting the battery from internal short circuits [5,6].

In current commercial LIBs, polyethylene (PE) and polypropylene (PP) are the most commonly used separators due to their affordability, chemical stability, and mechanical robustness. The electrochemical performance and safety of LIBs are significantly influenced by the separators' chemical properties, mechanical strength, and thermal stability [7]. A good separator should be chemically stable to prevent any side reaction with electrolyte and electrode materials at high or low temperatures and at higher working voltages. Additionally, the separator must be durable enough to withstand the tension generated during repeated charge-discharge cycles [8]. The ionic conductivity of a separator depends on its porosity and wettability, with uniformly distributed porosity being essential to prevent the growth of lithium dendrites on the anode surface [9,10]. Therefore, it is crucial to select raw materials that meet all the key characteristics required for an effective separator.

Several studies have been conducted to improve the porosity and wetting properties of separators, as well as their thermal stability [6]. Non-woven membranes, a type of separator made from natural or synthetic fibers, are prepared using methods such as melt-blowing, wet-laying, or electrospinning [6,11,12]. Various membranes with porosities ranging from 60 % to 80 %, pore sizes from 20 to 100 nm, and thicknesses from 100 to 200 μm have been synthesized using polymers like polyacrylonitrile (PAN), polyimide (PI), polymethyl methacrylate (PMMA), and polyvinyl alcohol (PVA) [13]. The diameter of a membrane's fibers determines its thickness and smoothness, which, in turn, contributes to its electrochemical stability, high porosity, and enhanced absorption rate. However, large pores, poor mechanical strength, and difficulties in thinning the coating can hinder effective isolation of the cathode and anode, potentially leading to short circuits. Significant progress has been made in recent years through surface engineering of separators to increase porosity, wettability, and chemical and thermal stability [14,15]. Composite membranes, created by stacking or modifying non-woven membranes with different materials, have also been explored in recent years. By combining organic and inorganic materials with polymers, these composite membranes can exhibit the physical and chemical properties needed to function as effective isolation membranes for LIBs [16–18].

For instance, Cai et al. [19] developed a novel PVDF-HFP/PI electrospun separator with a double-layer structure for high-performance LIBs. The double-layer polymer fibers not only combine the advantages of PVDF-HFP and PI but also improve the mechanical strength of the electrospun nonwoven fabric, resulting in a high porosity of up to 85.9 %. Their membranes showed excellent properties, including thermal stability (up to 200 °C), excellent liquid electrolyte absorption (483.5 %), and good ionic conductivity (*ca.* 1.78×10^{-3} S cm^{-1}). The PVDF-HFP/PI composite membrane-containing cell maintained a discharge capacity of approximately 118.2 mAh g^{-1} with a capacity retention of 98.1 %, which is significantly greater than that of the Celgard 2320 separator (94.9 %). Liu et al. [20] used the electrospinning method to prepare a PU/PVDF composite separator and used it in a $LiCoO_2$ (LCO) cathode and graphite anode in the LIB system. In comparison to cells employing commercial Celgard separators, the PU/PVDF membrane demonstrated stable discharge capacities over 100 cycles at a 0.2C rate. The PU/PVDF membrane also exhibited high porosity and mechanical strength, resulting in superior absorption rate and excellent ionic conductivity. Inorganic ceramic fillers such as Al_2O_3 and SiO_2-modified PVDF composite membranes were prepared by a melt-electrospinning and magnetron sputtering deposition method and reported by Wu et al. for high-power and high-safety LIBs [21]. The Al_2O_3/SiO_2/PVDF composite membranes exhibited greater porosity (61.8 %), better ionic conductivity (*ca.* 2.06×10^{-3} S cm^{-1}) and higher electrolyte uptake (366.0 %) than did the commercial PE separators. Compared to the PE separator (49.8 %), the Al_2O_3/SiO_2/PVDF membranes with Ni-rich cathode-based cells maintained a better capacity retention of 58.4 % at 8 C. An LATP ceramic filler containing a PVA/melamine composite nonwoven (LATP/PVAM) membrane was also reported by our group using electrospinning technology [22]; this material has several advantages, including high porosity (83.0 %), electrolyte uptake (214.0 %), ionic conductivity (*ca.* 1.77×10^{-3} S cm^{-1}) and excellent thermal stability (150 °C). The LATP/PVAM composite membrane was applied in an LIB system consisting of a $LiNi_{0.5}Mn_{1.5}O_4$ cathode and a $Li_4Ti_5O_{12}$ anode. The full cell based on our homemade LATP/PVAM composite membrane exhibited approximately 98.0 % capacity retention compared to that of the commercial PE separator (~93.0 %) at a high current (1C) rate for 100 cycles. The results indicate that the advantages of these composite separators are high porosity, low thermal shrinkage, good electrolyte uptake, and superior ionic conductivity.

The dip-coating strategy has recently been used for composite separator modification and is potentially useful for various applications, including wastewater treatment and LIB separator modification [23–26]. Specifically, a separator coated with a polymer or polymer dispersed with inorganic fillers can significantly enhance porosity, mechanical and thermal stability, and wettability to the electrolyte. This improvement facilitates superior transport of Li^+ ions, thereby enhancing electrochemical performance. For example, Wang et al. [27] reported a dip coating method to coat PVDF polymers on PE separators to prepare PE−PVDF composite membranes, which had excellent porosity (61.4 %), superior electrolyte wettability, and very good ion conducting (*ca.* 1.53×10^{-3} S cm^{-1}) properties. The PE−PVDF membranes exhibited better electrochemical performance, especially at high current rates such as 2C and 5C, which is mainly due to the excellent compatibility of the PVDF polymer with organic electrolytes [28]. Wu et al. [24] developed an ultrafine PVDF nanofiber membrane via a tip-induced electrospinning technique, followed by a dip-coating process using an Al_2O_3-containing polymer electrolyte solution, and explored it as a highly safe composite membrane for LIBs. The corresponding PVDF/Al_2O_3 composite membrane exhibited excellent properties, including porosity (55.8 %), electrolyte uptake (152.0 %), ionic conductivity (*ca.* 2.23×10^{-3} S cm^{-1}), thermal stability (140 °C), and capacity retention at 4 C with low discharge capacity loss. Chen

et al. [29] also fabricated an LIB cell using polyacrylonitrile (PAN) nanofibrous membranes through an electrospinning method and then dip-coated it with zeolite (ZSM-5) and phenoxy resin. The ZSM-5/PAN composite membranes demonstrate excellent thermal stability (180 °C) and high ionic conductivity (*ca.* 2.16 × 10^{-3} S cm^{-1}). The $LiFePO_4$-based half-cell based on the ZSM-5/PAN membrane shows a very impressive discharge capacity (102 mAh g^{-1}) at 7 C. Hence, the above findings in the literature suggest that the use of thin nanofiber composite membranes with a dip-coating strategy will be an effective way to operate LIBs at high temperatures and under harsh high current rate conditions.

The objective of this study was to fabricate a nanofibrous poly(vinyl alcohol)-melamine nonwoven membrane using electrospinning techniques and subsequently dip-coat the membrane with a PVDF polymer solution at various weight percentages. This material is referred to as Dip x% PVDF@Esp-PVAM (x = 1 % and 3 %) and can be used as a composite separator in highly safe LIB applications. Esp-PVAM nanofibers coated with thin and homogeneous PVDF layer are expected to enhance the performance of LIBs. In addition to its cost-effectiveness and environmentally friendly characteristics, PVA is renowned for its versatility and exceptional chemical and mechanical stability. The incorporation of melamine into electrospun nonwoven membranes has been demonstrated to enhance their thermal stability, making them suitable for high-temperature battery applications. Moreover, PVDF exhibits a strong affinity for liquid electrolytes, enhancing electrolyte wettability and facilitating the diffusion of Li^+ ions within the electrolyte. However, the amount of percentage of PVDF is a key factor to consider as a coating layer. If the coating layer is too thick, then it might adversely affect the performance of the membrane whereas a very thin layer might not be enough as a conductive coating layer on the membrane. Hence, optimizing the PVDF amount becomes a high priority.

SEM and FTIR analyses of the electrospun membranes confirmed their surface morphology and hierarchical structure. Our fabricated Dip 1%PVDF@Esp-PVAM composite separator exhibits outstanding electrolyte uptake, thermal stability, and porosity. These properties enable the separator to operate effectively across a wide range of voltages while enhancing lithium-ion conductivity. The half-cell, utilizing the $LiNi_{0.8}Co_{0.1}Mn_{0.1}O_2$ (NCM811) cathode material and the as-prepared Dip 1%PVDF@Esp-PVAM membrane was directly compared with conventional PE separator to demonstrate the improved performance of the home-made 1%PVDF@Esp-PVAM membrane. Additionally, the thermal stability of the membrane enables it to operate over a wide range of voltages, which allows for more efficient charging and discharging of the battery. Our proposed Dip 1%PVDF@Esp-PVAM composite separator has also

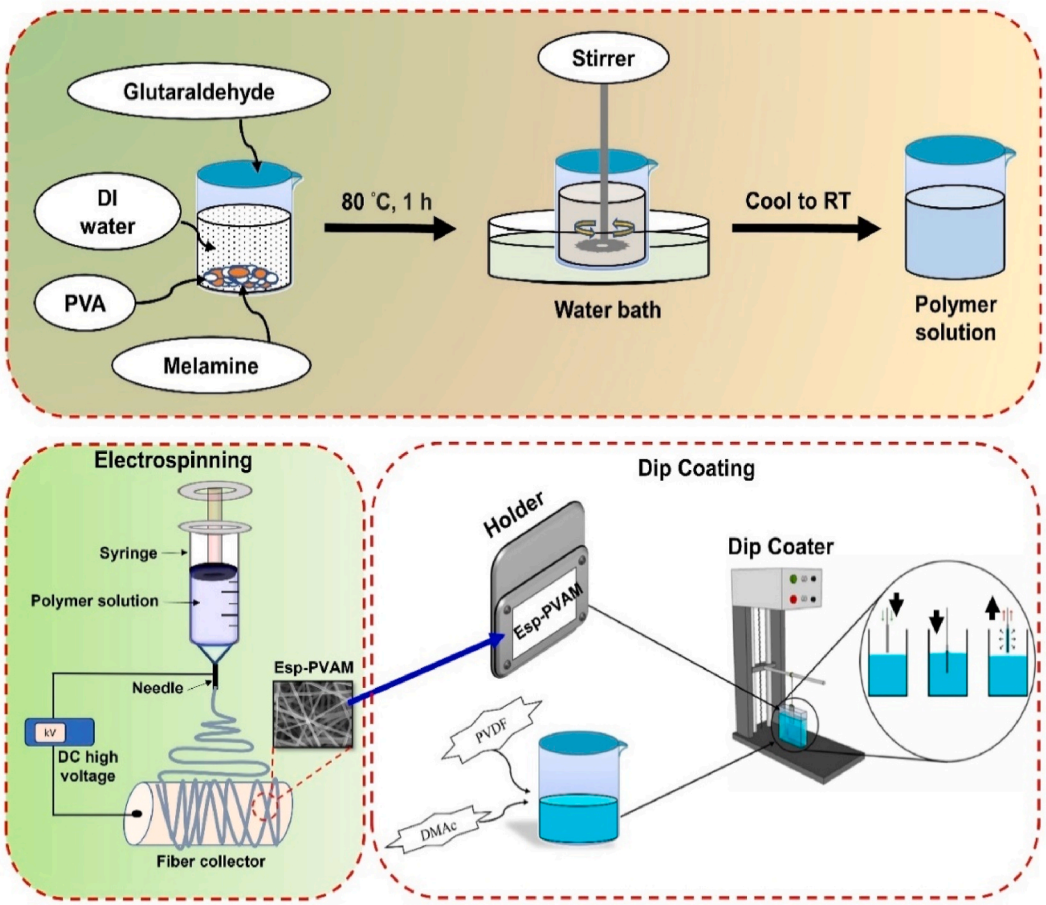

Scheme 1. Schematic representation of the preparation of nonwoven Esp-PVAM composite membranes using dip-coating method with PVDF polymer solution.

been demonstrated to be scalable for high-safety and high-power LIB applications.

2. Experimental

2.1. Preparation of PVDF dip-coated Esp-PVAM nonwoven separators

The polymer solution was prepared by adding 1.95 g PVA to 18 mL of deionized water which already contains 0.05 g of melamine and 2.5 g of glutaraldehyde (GA). This mixture solution was stirred at 80 °C until it became milky white. After cooling to room temperature, the resultant polymer solution was electrospun with an electrospinning machine (NANON-01A, Japan) at 25–30 kV. The distance from the needle to the collection plate was 25 cm and the needle is composed of stainless steel, model 23 (inner diameter 0.33 mm, outer diameter 0.63 mm, tube diameter and thickness 0.15 mm). The flow rate was set to 1 mL h^{-1}, with a solution volume of 4 mL. The positive electrode was connected to a high-voltage needle, the negative electrode was connected to the collection plate, and aluminum foil was used to collect the spun fibers from the electrospinning instrument. Later, the obtained fiber membrane was ripped off the aluminum foil and pasted on a paper fixed to a glass plate, and heated to 90 °C.

The PVDF soaking solution was prepared by dissolving the PVDF powder in DMAc at varying concentrations (e.g., 1 wt% and 3 wt% PVDF). Then the as-fabricated polymer membrane was dipped in to the solution prepared above by using a custom fixture holding the electro-spun nanofiber membrane in a dip-coating machine at the speed of 400 mm min^{-1}. The membrane was dipped three times with dipping time of 10 s each. Finally, the PVDF-impregnated nonwoven membranes were allowed to dry at 60 °C for a period of 12 h followed by cutting them into circular discs with a diameter of 16 mm and used as is. In Scheme 1, a schematic diagram is shown that illustrates the preparation of electrospun PVAM nonwoven membranes and the dip-coating process. Hereafter, the corresponding as-prepared nonwoven membranes are referred to as the pristine Esp-PVAM, Dip 1 % PVDF@Esp-PVAM, and Dip 3 % PVDF@Esp-PVAM composite membranes. These membranes are produced with a thickness of *ca.* 20 μm, the same thickness as popular membranes (16 μm), as shown in Table S1. The as-prepared nanofiber composite separators were then placed in an Ar-filled glove box for further studies.

2.2. Ni-rich NCM811 electrode preparation

During the preparation of the cathode, the NCM811 cathode material, PVDF, and Super P were weighed 80:10:10 (in weight percent), and the solid content was controlled at 30 %. A mixture of 2 g of NCM811 cathode material and 0.25 g of Super P were ground in a mortar and heated at 120 °C for 1 h to remove excess moisture. In addition, 3.57 g of 7 wt% PVDF in NMP binder solution was precisely weighed in a beaker, together with 2.51 g of N-methyl pyrrolidone (NMP) as organic solvent, which was then stirred using a DC motor stirrer at a speed of 150 rpm for 15 min. The dried and dehydrated active material powder was slowly added to the PVDF/NMP solution and stirred gently at 450 rpm for 3 h and then at a slower speed of 150 rpm for 1 h. The homogeneous slurry was coated on aluminum foil using the doctor blade coating method with a wet thickness of 200 μm and placed in an oven at 80 °C for 4 h to volatilize the organic solvent. The dried electrode was flattened with a roller, and a 13 mm round cutter was used to cut pieces of circular discs for storage in a glove box for further experiments. The average cathode material loading was controlled at *ca.* 3 mg cm^{-2}.

2.3. Materials and electrochemical Characterization

X-ray diffraction (XRD) was conducted with a Bruker D2 Phaser (Germany). Scanning electron micrographs (SEM) of the materials were obtained using a Hitachi S–2600H (Japan) instrument. A PerkinElmer Spectrum 100 (USA) analyzer was used to perform Fourier transform infrared (FTIR) spectroscopy and a thermogravimetric analyzer (Mettler, USA) was used to conduct thermogravimetric analysis (TGA) and differential scanning calorimetry (DSC) at temperatures between 25 °C and 600 °C at a heating rate of 5 °C min^{-1}. In this study, linear sweep voltammetry (LSV) was performed using a Metrohm Autolab PGSTAT32 N in the potential range of 0–5.5 V (*vs.* Li/Li^+) at a scanning rate of 0.001 V s^{-1}. The electrochemical impedance spectroscopy (EIS) data of the cells were obtained using a Metrohm Autolab PGSTAT32 N in the frequency range $10^6 \times 10^{-2}$ Hz and at an amplitude of 5 mV. These measurements were always conducted using a standardized OCP. A BioLogic BCS-805 (France) was used for chronoamperometry and AcuTech Systems BAT-750B (Taiwan) battery tester was used to measure the charge/discharge characteristics of the cells at room temperature within the voltage range of 2.5–4.3 V (*vs.* Li/Li^+), and 1C was set to 20 mA g^{-1}. A Neware battery tester (China) was used to analyze symmetric cells.

2.4. Electrolyte uptake (A%) measurement

This experiment aimed to evaluate the absorption and swelling of the membrane under saturated solution conditions using the weighing method. A homemade electrospun nonwoven membrane served as the experimental sample. Initially, the membrane was dried at 60 °C for 12 h to determine its dry weight (W_{dry}). Subsequently, the membrane was immersed in 1 M $LiPF_6$ in EC/DEC (1:1 vol ratio) electrolyte for 12 h. After removing the membrane and gently blotting it with lens paper to absorb surface liquid, the wet weight (W_{wet}) was measured. The electrolyte uptake (A%) can be calculated using Eqn. (1) as follows:

$$A\% = \frac{W_{wet} - W_{dry}}{W_{dry}} \times 100\ \% \quad (1)$$

2.5. Porosity (P%) measurement

The porosity of the nonwoven membrane was determined by the amount of solvent absorbed by the film. The as-prepared membrane was initially dried in an oven at 60 °C for 12 h to remove moisture and achieve dryness. After drying, the film thickness and dry weight were measured. In the next step, the composite membrane was immersed in n-butanol for 12 h. Excess liquid on the surface was carefully removed using dust-free test paper, and the wet weight was then measured. The porosity (P%) of the isolation film can be calculated using experimental data according to Eqn. (2).

$$P\% = \frac{M_{BuOH}/\rho_{BuOH}}{M_{BuOH}/\rho_{BuOH} + M_m/\rho_p} \tag{2}$$

where P is the porosity (%) of the membrane, M_{BuOH} is the absorption capacity of n-butanol by the membrane (g), ρ_{BuOH} is the density of n-butanol (0.8098 g cm^{-3}), M_m is the dry film weight (g), and ρ_p is the density of the pristine membrane.

2.6. Mechanical stability measurement

The mechanical strength of the as-prepared composite membranes was examined by a tensile tester (EZ-LX 500 N). The membrane was cut into test pieces (8 cm × 1 cm) and then clamped to the tensile tester to be stretched until it tore away with a stretching speed of 2 mm s^{-1}. The stress and strain of the composite membrane were obtained through the following Eqns. (3) and (4):

$$\text{Stress } (\sigma) = \frac{\text{load (Kgf)}}{\text{thickness(mm)} \times \text{width(mm)}} \tag{3}$$

$$\text{Strain } (\%) = \frac{\text{displacement(mm)}}{\text{initial length(mm)}} \times 100 \tag{4}$$

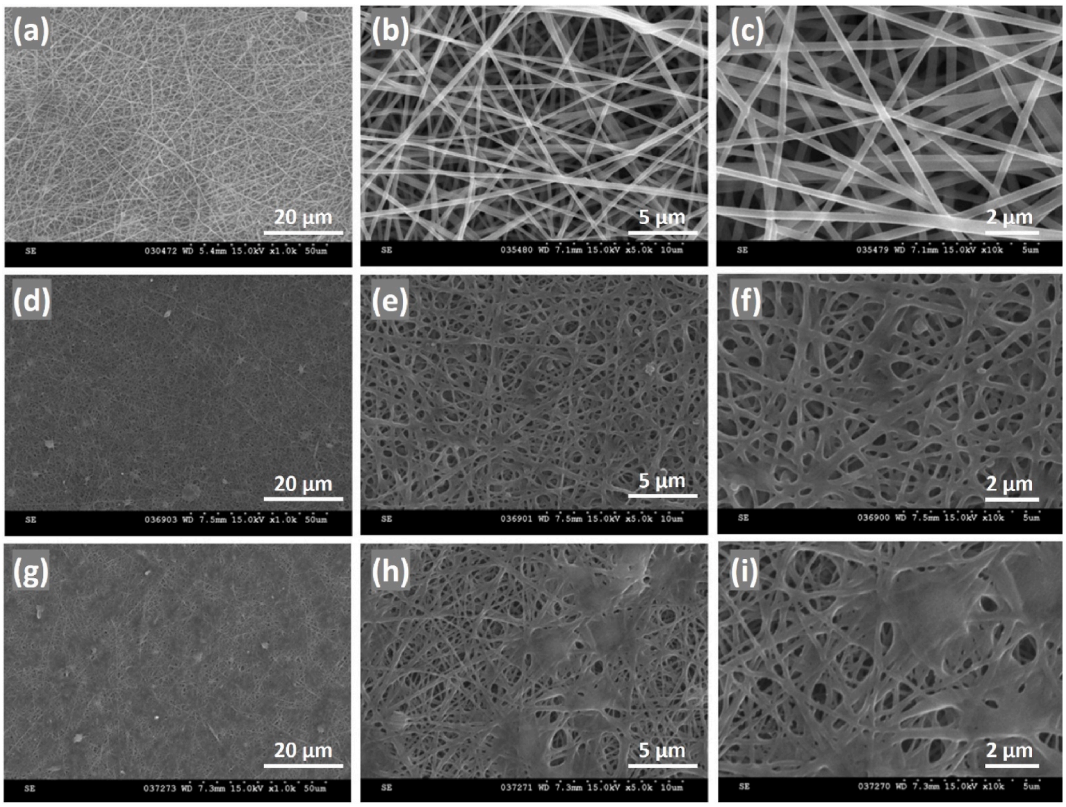

Fig. 1. Low- and high-magnification SEM images of the (**a-c**) Esp-PVAM, (**d-f**) Dip 1 % PVDF@Esp-PVAM, and (**g-i**) Dip 3 % PVDF@Esp-PVAM nonwoven composite separators.

2.7. Ionic conductivity Investigation

A custom-built device was utilized to measure the lithium-ion conductivity of the composite membranes in this study. Before the experiment, the composite membranes were immersed in 1 M $LiPF_6$ in EC/DEC (1:1) electrolyte for 12 h to ensure complete saturation. Excess electrolyte was carefully removed using clean paper. Subsequently, the membranes were positioned in the center of the ion conductivity measuring instrument and securely fixed between metal electrodes. These electrodes featured gold-plated surfaces and served as the working electrode and counter electrode, respectively. The entire setup was placed in a constant temperature oven, and a fixed amplitude of 5 mV was applied for the conductivity measurement. The scanning frequency range for impedance spectroscopy was set between 1 MHz and 100 Hz, and the temperature varied across a range from low to high values. Measurements were performed under different temperature conditions: 20, 30, 40, 50, and 60 °C. From the electrochemical impedance spectroscopy (EIS) results, the overall impedance value (R_b) of the membrane was determined at the Z′ value corresponding to the highest frequency. This R_b value was then used in Eqn. (5) to calculate the lithium-ion conductivity (σ_i).

$$\sigma_i = \frac{L}{R_b \times A} \tag{5}$$

where σ_i is the ionic conductivity (S cm^{-1}), L is the thickness (cm), R_b is the AC overall resistance value (ohm), and A is the cross-sectional area of the electrode clamp (a metal rod with a diameter of 1.3 cm).

3. Results and discussion

The surface morphologies of the homemade electrospun bare PVAM membrane and the composite membrane impregnated with PVDF polymer were examined using SEM analysis. Fig. 1(a)-(c) reveal densely distributed fibers with a uniform diameter of approximately 250 nm and large pores in the bare PVAM membrane. In Fig. 1(d)–(i), a distinct PVDF polymer coating layer is visible on the surface of the electrospun PVAM nanofibers, where the fiber diameter increases from 250 to around 500 nm with increasing PVDF content. Consequently, as the PVDF polymer coating increases, the membrane pores tend to decrease gradually. Thus, the Dip 1 % PVDF@Esp-PVAM composite separator demonstrates a more uniform pore size distribution compared to the Dip 3 % PVDF@Esp-PVAM composite separator. The former exhibits higher porosity and excellent electrolyte wettability.

The pore size distribution of a separator or membrane plays a crucial role in overall performance of a battery. To ensure smooth transport of lithium ions during charging and discharging, it is essential for the composite membrane to have an optimal pore size that prevents ion hindrance or membrane puncture due to excessively large pores. We analyzed the pore size distribution of various homemade electrospun PVAM composite separators using a porous material analyzer (PMI), with results depicted in Fig. 2. Fig. 2(A) illustrates the pore size distribution of the pristine Esp-PVAM composite separator, showing uniform pores with an average size of approximately 1186 nm. In contrast, Fig. 2(B) shows that the average pore size of the Dip 1 % PVDF@Esp-PVAM composite separator was reduced by half to about 533–600 nm after PVDF polymer coating. This indicates successful pore size reduction without pore clogging. Furthermore, increasing the PVDF polymer coating to 3 wt% significantly decreased the average pore size further. Fig. 2(C) displays that the Dip 3 % PVDF@Esp-PVAM composite separator has an average pore size of approximately 318 nm. This optimized pore size is beneficial for enhancing long-term lithium-ion transport efficiency.

FTIR analysis was conducted to verify the presence of PVDF coating on the Esp-PVAM nonwoven composite separator, with results depicted in Fig. 3(A). The spectrum of the Esp-PVAM composite separator (Fig. 3(A), curve a) exhibits characteristic peaks at 3308.33, 2939.81, 1712.61, 1327.51, and 1087.35 cm^{-1}, corresponding to vibrations of O–H, C–H, C═O, C–O, and C–C bonds, respectively. Fig. 3(A) curves b and c illustrate the FTIR spectra of the Dip 1 % PVDF@Esp-PVAM and Dip 3 % PVDF@Esp-PVAM composite separators, respectively. In these spectra, characteristic peaks of PVDF polymer are observed at 801.38–840.36 cm^{-1}, 1177.19–1179.17 cm^{-1}, and 1142.43–1143.02 cm^{-1}, which correspond to vibrations of $–CH_3$, $–CF_2$, and $–CF_2$ groups, respectively. The intensity of these absorption peaks increases notably with higher PVDF concentration, indicating successful coating of PVDF onto the Esp-PVAM nonwoven composite separator.

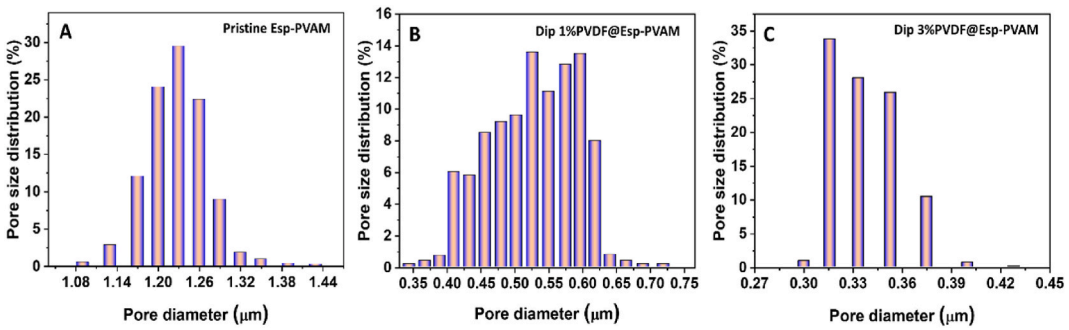

Fig. 2. Pore size distribution analysis of (**A**). Pristine Esp-PVAM, (**B**). Dip 1 % PVDF@Esp-PVAM, and (**C**). Dip 3 % PVDF@Esp-PVAM nonwoven composite separators.

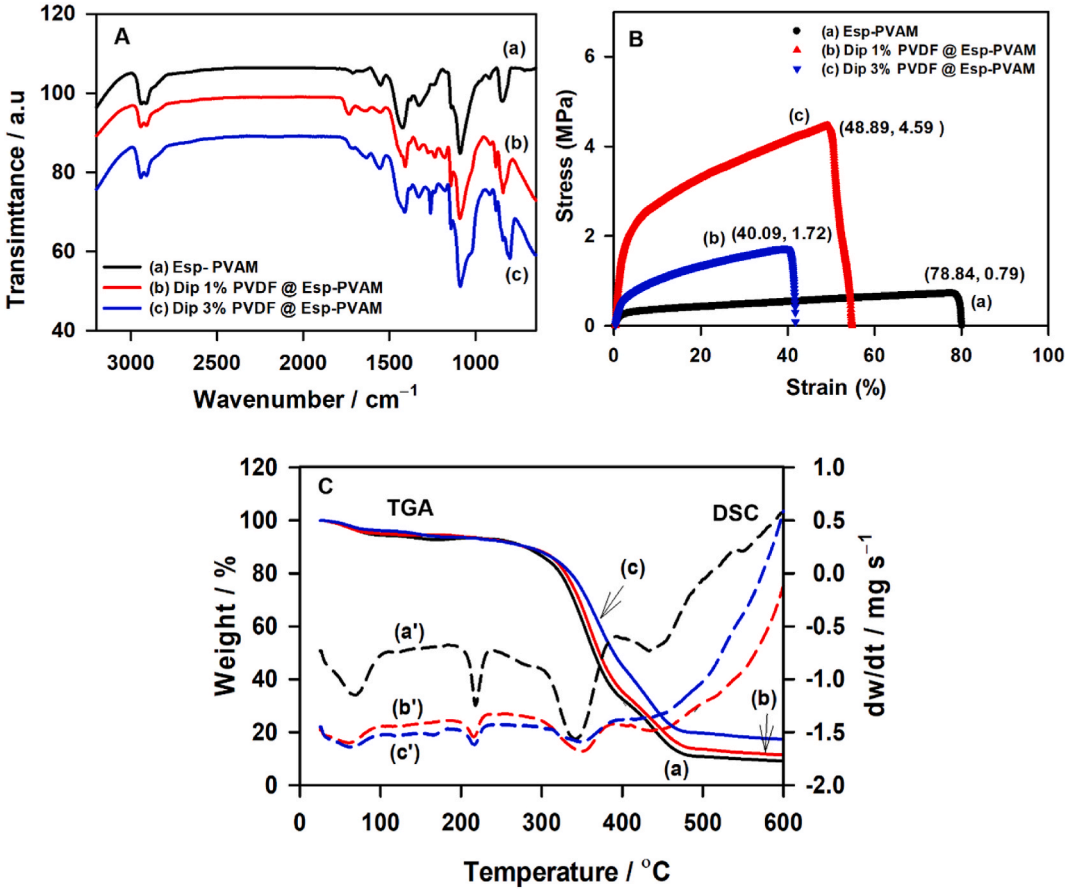

Fig. 3. **(A)** FTIR, **(B)** stress−strain, and **(C)** TGA (solid lines; a-c) and DSC (dotted lines; a'-c') curves of (a). Pristine Esp-PVAM, (b). Dip 1 % PVDF@Esp-PVAM, and (c). Dip 3 % PVDF@Esp-PVAM nonwoven composite separators.

Most nonwoven membranes or separators used in lithium-ion batteries exhibit porous structural characteristics. During the extended charge-discharge cycles, the separator must not only possess excellent electrolyte absorption and wetting properties to enable free movement of Li^+ ions between electrodes but also exhibit high thermal stability. Equally important is the requirement for sufficient mechanical strength in the separator. The tensile strengths of the pristine Esp-PVAM, Dip 1 % PVDF@Esp-PVAM, and Dip 3 % PVDF@Esp-PVAM composite separators were evaluated using a tensile tester instrument, with corresponding data presented in Fig. 3 (B). The incorporation of PVDF into the Esp-PVAM composite separator resulted in increased elongation tendencies. The micropore size and distribution within the composite membrane significantly influenced its tensile strength. It is evident that electrospun PVAM impregnated with a PVDF polymer layer enhances mechanical strength.

DSC (Differential Scanning Calorimetry) and TGA (Thermogravimetric Analysis) analyses were conducted to assess the thermal stability of the pristine and PVDF-coated Esp-PVAM composite separators, as depicted in Fig. 3(C). The DSC curve (dotted lines) reveals parameters such as glass transition temperature (T_g), melting point (T_m), and decomposition temperature of the composite separator. Meanwhile, the TGA curve (solid lines) illustrates the weight loss of the composite separator with increasing temperature. These analyses provide insights into the thermal characteristics and stability of the separators, crucial for their performance in LIB applications.

The TGA analysis showed that as the concentration of PVDF impregnation increased, the residual content of the Esp-PVAM composite separator also increased after exposure to high temperatures up to 600 °C. In the DSC curve, several distinct peaks were observed. The first small peak, occurring between approximately 40 to 120 °C, is attributed to the release of absorbed free water from the membrane. The second peak, evident between 180 and 280 °C, displays an endothermic peak around 240 °C. The third decomposition phase, occurring between 350 and 550 °C, shows significant peak variations, corresponding to the initial decomposition of PVA. As the temperature increases, PVA chains gradually decompose and form polyene structures, which further break down into lower molecular weight substances [30]. Comparatively, the DSC curves of the pristine Esp-PVAM composite separator exhibit more pronounced heat absorption signals across these three peaks than those of the PVDF-coated composite separator. This indicates that the PVDF coating layer effectively enhances the thermal stability of the Esp-PVAM composite separator.

The liquid uptake and porosity of our homemade nonwoven composite separators, including pristine Esp-PVAM, Dip 1 % PVDF@Esp-PVAM, and Dip 3 % PVDF@Esp-PVAM membranes, were studied and compared with those of a commercial PE separator

(Table S1). Comparing the results, the pristine Esp-PVAM composite separators exhibit approximately 446.8 % liquid uptake and 58.4 % porosity, both higher than those of commercially available PE separators. These characteristics are attributed to PVAM, which enhances the cell's electrochemical performance by enabling high liquid uptake through electrospun nanofiber membranes. Furthermore, the liquid uptake and porosity of the Esp-PVAM composite separator, coated with PVDF polymer, increase with higher impregnation concentrations. This underscores how PVAM membranes when coated with PVDF, effectively enhance the liquid uptake and porosity of the composite separator.

Using a contact angle analyzer, we studied the electrolyte wettability of commercially available PE separators and homemade PVAM nonwoven composite separators. The experiment employed a 1 M $LiPF_6$ in EC/DEC (1:1) electrolyte solution, dispensed onto the separators and measured for their contact angles. A smaller contact angle indicates better wetting of the separator by the electrolyte. Fig. 4(A)–(D) illustrate that the contact angles for the (A) PE separator, (B) Esp-PVAM, (C) Dip 1 % PVDF@Esp-PVAM, and (D) Dip 3 % PVDF@Esp-PVAM composite separators were approximately 73.9°, 21.4°, 46.8°, and 48.8°, respectively. The results indicate that as the PVDF coating concentration increases, the contact angle of the Esp-PVAM composite separators also increases, correlating with a reduction in membrane pore size. This slower electrolyte wetting due to smaller pores leads to higher contact angles for PVDF-coated Esp-PVAM separators compared to PE separators. Conversely, the smaller pores enhance the composite membrane's porosity, promoting better electrolyte wettability and longer moisture retention. This characteristic is advantageous for improving the long-term cycling stability.

For thermal shrinkage evaluation, both a PE separator and Esp-PVAM composite separators were subjected to heating from 50 °C to 200 °C, with a subsequent 30-min hold at 200 °C. Fig. 5(A)–(D) depict the dimensional changes (shrinkage) observed in the PE separator, pristine Esp-PVAM, Dip 1%PVDF@Esp-PVAM, and Dip 3%PVDF@Esp-PVAM composite separators before and after heat treatment. At 200 °C, the commercially available PE separator exhibited a higher shrinkage rate compared to the pristine Esp-PVAM and PVDF-coated Esp-PVAM composite separators. However, the PVDF-coated Esp-PVAM composite separators also showed some degree of shrinkage. Specifically, the analysis indicated that while the PE separator exhibited the most noticeable shrinkage percentage at 200 °C, the PVDF-coated Esp-PVAM composite separators experienced significantly less shrinkage compared to the pristine Esp-PVAM membrane. This result suggests that the presence of PVDF reduced the shrinkage propensity of the composite separators, likely due to the lower crystallinity of PVDF at elevated temperatures.

Specifically, the Esp-PVAM composite separators with 3 % PVDF polymer experienced more shrinkage (approximately 29 %) compared to those with 1 % PVDF polymer (around 12 %), reflecting the influence of PVDF polymer concentration on thermal behavior. In conclusion, the optimized Dip 1%PVDF@Esp-PVAM composite separators demonstrated excellent mechanical strength and reasonable thermal properties (shrinkage percentage), highlighting their suitability for safe and efficient applications in LIBs.

Temperature-dependent lithium-ion conductivity measurements of the prepared nonwoven composite separators were conducted using a custom-built apparatus. The electrolyte used was 1 M $LiPF_6$ in EC/DEC (1:1). Various separators including the PE separator, pristine Esp-PVAM, Dip 1%PVDF@Esp-PVAM, and Dip 3%PVDF@Esp-PVAM composite separators were tested across temperatures ranging from 25 to 70 °C. Table S2 shows that the ionic conductivities of the PE separator, pristine Esp-PVAM, Dip 1%PVDF@Esp-

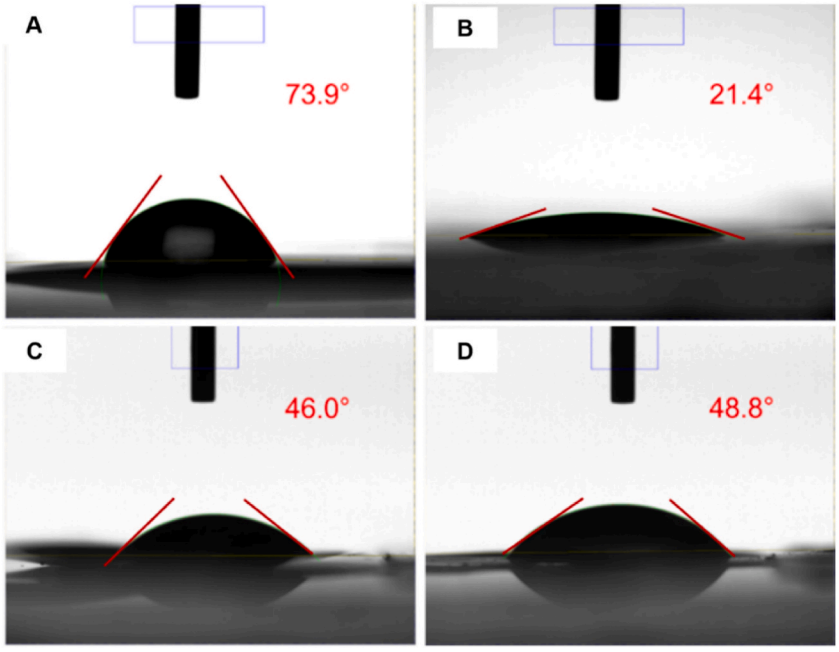

Fig. 4. Photograph of contact angle measurements of **(A)** PE, **(B)** Esp-PVAM, **(C)** Dip 1 % PVDF@Esp-PVAM, and **(D)** Dip 3 % PVDF@Esp-PVAM composite separators.

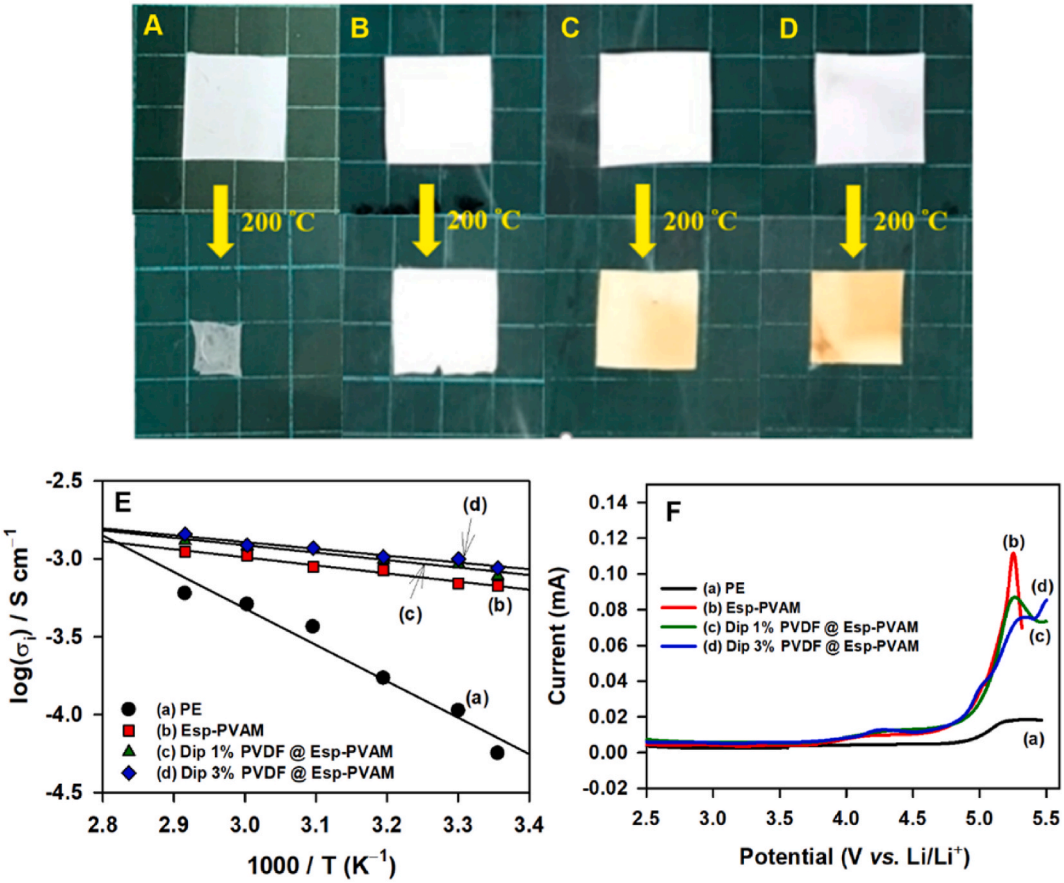

Fig. 5. Photographs of the thermal shrinkage of the **(A)** PE, **(B)** pristine Esp-PVAM, **(C)** Dip 1%PVDF@Esp-PVAM, and **(D)** Dip 3%PVDF@Esp-PVAM composite separators at 200 °C, **(E)** Thermally dependent ionic conductivity measurements, and **(F)** LSV curves of the different composite separators.

PVAM, and Dip 3%PVDF@Esp-PVAM composite separators are approximately 5.65×10^{-5}, 6.71×10^{-4}, 7.75×10^{-4} and 8.74×10^{-3} S cm^{-1}, respectively, at 25 °C. At 70 °C, the ionic conductivities are approximately 6.01×10^{-4}, 1.11×10^{-3}, $1.31 \times 10^{-3,}$ and 1.44×10^{-3} S cm^{-1}, respectively. Fig. 5(E) shows the Arrhenius plots of different composite separators in 1 M $LiPF_6$ in an EC/DEC (1:1) electrolyte. The activation energy (E_a) can be calculated based on the slope of the linear plot in Fig. 5(E). The estimated E_a of the PE separator is approximately 44.75 kJ mol^{-1}, whereas the E_a values of the pristine Esp-PVAM, Dip 1%PVDF@Esp-PVAM, and Dip 3% PVDF@Esp-PVAM composite separators are approximately 9.89, 9.12, and 8.35 kJ mol^{-1}, respectively. The experimental findings demonstrate that compared to commercial PE separators, our homemade pristine Esp-PVAM, Dip 1%PVDF@Esp-PVAM, and Dip 3% PVDF@Esp-PVAM composite separators exhibit higher ionic conductivity and significantly lower activation energy. These improvements are primarily attributed to the enhanced liquid electrolyte uptake and superior wettability properties of our composite membranes. Furthermore, all PVDF-coated Esp-PVAM composite separators show higher lithium-ion conductivity and lower activation energy (E_a) compared to the pristine Esp-PVAM membrane. This is due to the electron-withdrawing nature of the PVDF polymer's main chain (-CF_2 group), which accelerates lithium-ion transport within the electrolyte. Additionally, the Esp-PVAM membrane itself possesses high porosity and excellent wettability, further improved by PVDF impregnation. The reduction in pore size in PVDF-coated Esp-PVAM separators significantly enhances electrolyte retention. Combining these advantageous characteristics effectively enhances electrolyte retention and ionic conductivity, making these composite separators promising for future applications in LIBs.

To investigate the interface stability and electrochemical compatibility of the prepared composite separators with lithium metal, an asymmetric cell (stainless steel || separator || lithium metal) was assembled for Linear Sweep Voltammetry (LSV) testing at room temperature. Fig. 5(F) illustrates the electrochemical stability window of the different composite separators used in this study. Comparative analysis with the commercial PE separator reveals that pristine Esp-PVAM-based membranes exhibit slight oxidation around 4.9 V (*vs*. Li/Li^+). Additionally, Dip 3%PVDF@PVAM composite separators show oxidation reactions beginning at approximately 4.9 V (*vs*. Li/Li^+), attributed to electrolyte decomposition. These findings indicate that excessive PVDF polymer impregnation can lead to electrolyte breakdown at lower voltage levels. Optimally, Esp-PVAM composite separators with a balanced amount of PVDF polymer coating demonstrate enhanced electrochemical performance. The Li || separator || Li symmetric cell was prepared with commercial PE, pristine Esp-PVAM, Dip 1 % PVDF@Esp-PVAM, and Dip 3 % PVDF@Esp-PVAM composite separators to study the

polarization potential and durability of the membranes, as reported in Fig. S3. Compared to conventional PE and non-coated Esp-PVAM, the PVDF-impregnated PVAM membranes exhibited lower polarization and improved durability. This indicates that PVDF coating enhances the stability and performance of the Esp-PVAM composite separators in lithium-ion batteries.

The electrochemical performances of the as-prepared electrospun PVAM membranes, including pristine Esp-PVAM, Dip 1% PVDF@PVAM, and Dip 3%PVDF@PVAM composite separators, were tested, and their performances were compared with those of a commercially available PE separator. The NCM811 cathode and Li metal anode were assembled in a CR2032-type coin cell with different membranes in this work. All these cells were operated in the potential range between 2.5 and 4.3 V (*vs.* Li/Li^+) at a charge and discharge current rate of 0.1C/0.1C for 5 cycles. The analysis results are shown in Fig. 6(A) and (B). The initial coulombic efficiencies (ICE) and discharge capacities of the 2032-coin cells with various composite separators, such as (a) PE separator, (b) pristine Esp-PVAM, (c) Dip 1%PVDF@Esp-PVAM, and (d) Dip 3%PVDF@Esp-PVAM, are approximately 71.6, 81.2, 80.6, and 83.8 %, and 183.8, 196.5, 193.2, and 191.4 mAh g^{-1}, respectively. During the initial activation cycle, some overcharge occurred; however, after 5 cycles, the coulombic efficiencies (CEs) and discharge capacities of all cells stabilized. Notably, cells with pristine Esp-PVAM and PVDF-coated Esp-PVAM composite separators demonstrated superior electrochemical performance compared to those using PE separators. This improvement is attributed to the Esp-PVAM nanofiber membranes' excellent electrolyte uptake, wettability, and high porosity. These characteristics facilitate rapid Li^+ ion transport, contributing to enhanced electrochemical performance at a 0.1C discharge rate.

Fig. 6(C) shows the high-rate profiles of the cells based on the (a) PE separator, (b) pristine Esp-PVAM, (c) Dip 1%PVDF@Esp-PVAM, and (d) Dip 3%PVDF@Esp-PVAM composite separators charged at 0.2C and discharged at various rates of 0.2C, 0.5C, 1C, 3C, 5C, and 10C. The corresponding charge/discharge cycles are shown in Figs. S1(A)–(D). The calculated discharge capacities of the PVAM composite separators-based cells are summarized in Table S3. The cells based on the pristine Esp-PVAM and PVDF-coated Esp-PVAM composite separators showed higher discharge capacities than those based on PE at high C rates. However, the cell with the Dip 1%PVDF@Esp-PVAM composite separator exhibited the highest discharge capacities across all C-rates. In contrast, when the PVDF polymer content was increased to 3 wt%, the discharge capacities significantly decreased. This analysis indicates that an appropriate amount of PVDF polymer coating on the pristine Esp-PVAM membrane can reduce porosity and enhance the mechanical strength of the membrane, leading to markedly improved electrochemical performance. However, excessive impregnation blocks the pores of the nonwoven membrane, slowing lithium-ion transport and reducing discharge capacity. Therefore, the optimal surface modification for the Esp-PVAM composite separator is 1 wt% PVDF.

Fig. 6(D) displays the long-term cycling stability profiles of cells based on different separators: (a) PE separator, (b) pristine Esp-

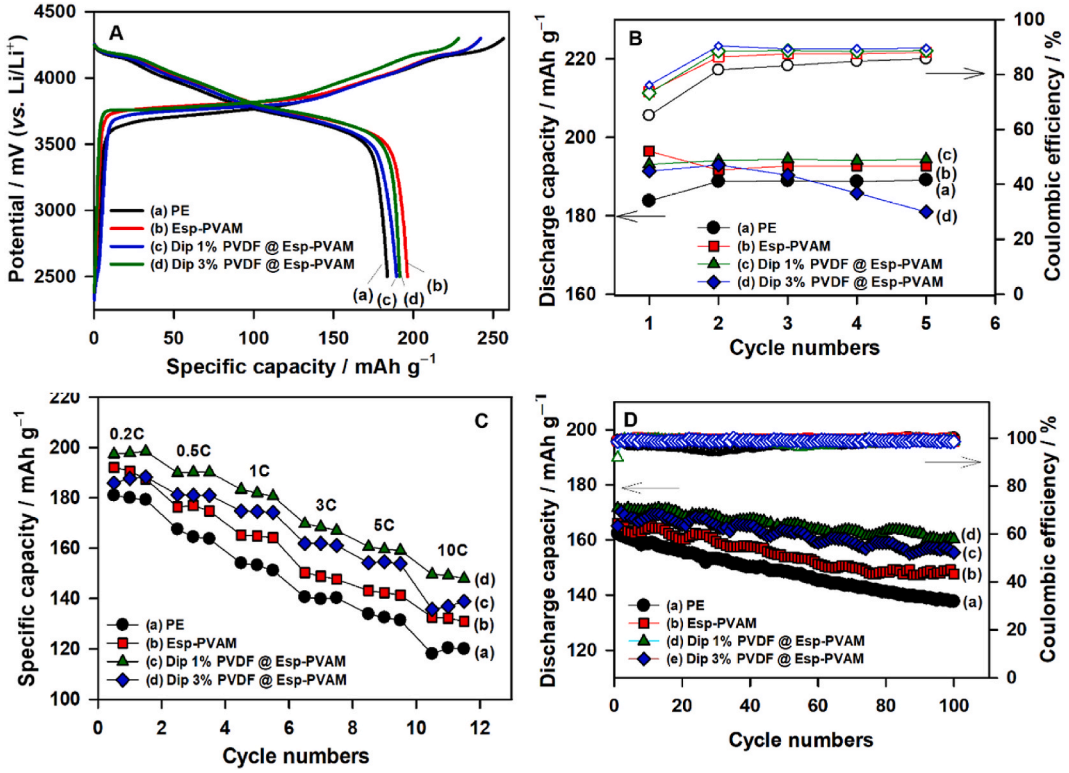

Fig. 6. Comparison of the electrochemical performances of different membranes, such as (a) PE, (b) pristine Esp-PVAM, (c) Dip 1%PVDF@Esp-PVAM, and (d) Dip 3%PVDF@Esp-PVAM composite separators: **(A).** Initial cycles at a 0. C, **(B).** Activation of 5 cycles at 0.1C, **(C).** high-rate profile in the range of 0.2C–10C rates, and **(D).** Long-term cycling stability test at 1C/1C for 100 cycles.

PVAM, (c) Dip 1%PVDF@Esp-PVAM, and (d) Dip 3%PVDF@Esp-PVAM composite separators. These cells underwent 100 charge and discharge cycles at a 1C/1C rate. The corresponding charge/discharge curves can be seen in Figs. S2A–D. After 100 cycles, the cells retained discharge capacities of approximately 153.2, 159.5, 160.3, and 155.4 mAh g^{-1}, respectively. The capacity retentions of these cells were approximately 80.8 %, 88.9 %, 93.4 %, and 91.3 %, respectively. From these results, the Dip 1%PVDF@Esp-PVAM composite separator provides the best cycling stability and capacity retention (160.3 mAh g^{-1} *vs.* 93.4 %), due to the balance of porosity and mechanical strength that facilitates efficient lithium-ion transport.

AC impedance analysis was performed on half-cells with different separators: (a) PE separator, (b) pristine Esp-PVAM, (c) Dip 1% PVDF@Esp-PVAM, and (d) Dip 3%PVDF@Esp-PVAM composite separators. Measurements were taken (A) before and (B) after long-term cycling tests at a 1C/1C rate. The corresponding data are shown in Fig. 7(A) and (B). Enlarged views of the high-frequency region are displayed in Fig. 7(C) and (D). The curves were fitted based on the AC impedance Circuit Model, with parameters including bulk impedance (R_b), charge transfer impedance (R_{ct}), total impedance (R_{total}), and Warburg impedance (Z_w). The equivalent circuit model is shown in the insets of Fig. 7(A) and (B).

Results indicate that cells with Esp-PVAM composite separators exhibit lower Rct (<50 Ω) during activation cycles, significantly lower than the cell with the PE separator. After 100 cycles at 1C/1C, the Dip 1%PVDF@Esp-PVAM composite separator demonstrated

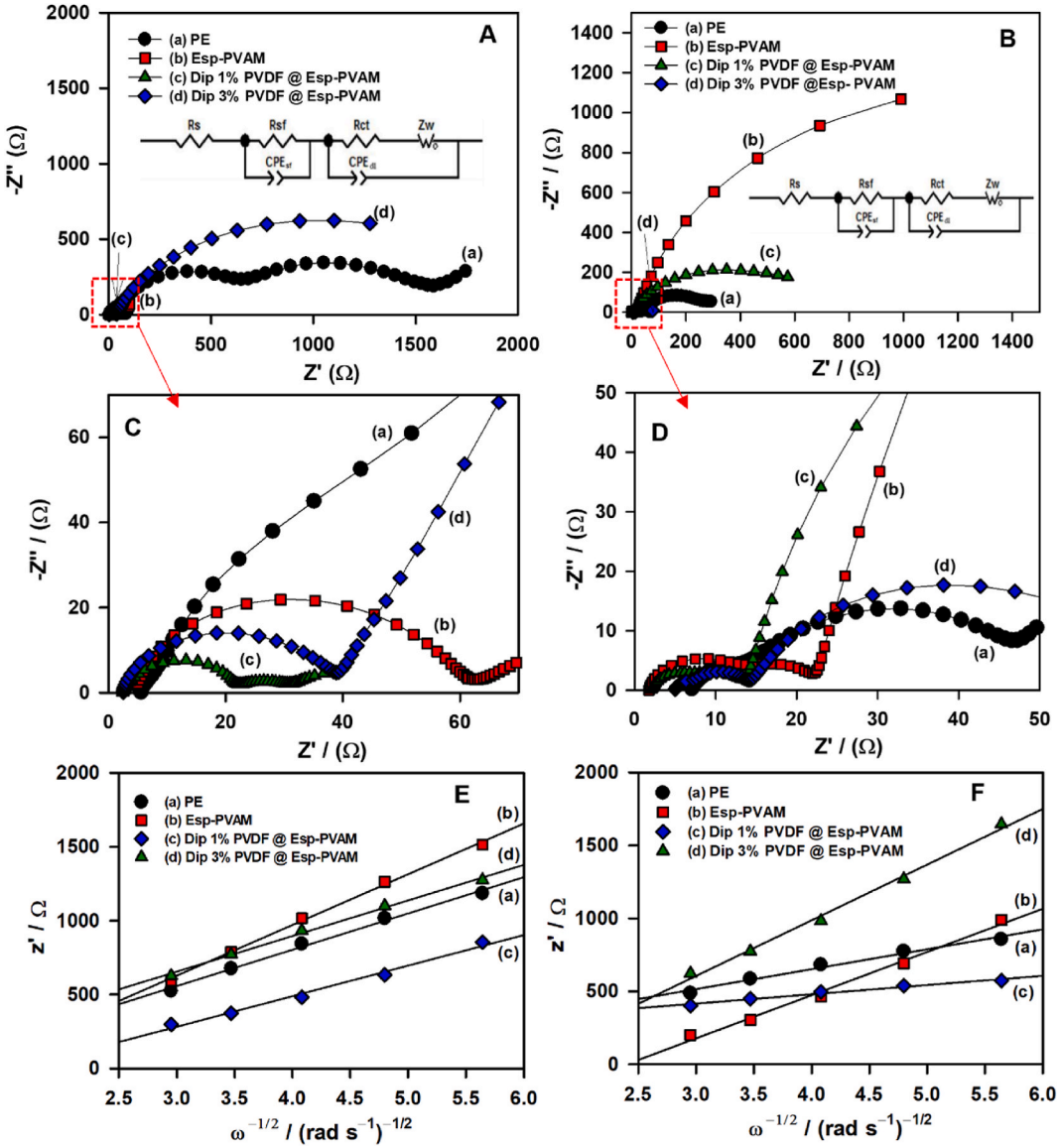

Fig. 7. Nyquist plots of the 2032 cells based on the (a) PE separator, (b) pristine Esp-PVAM, (c) Dip 1%PVDF@Esp-PVAM, and (d) Dip 3% PVDF@Esp-PVAM composite separators: **(A)** before and **(B)** after 100 cycles at a rate of 1C/1C; the high-frequency region is shown in **(C)** and **(D).** The corresponding linear relation of Z′ *vs.* $\omega^{-1/2}$ plot for the calculation of the lithium-ion diffusion coefficient (D_{Li}^{+}) in (E) and (F).

the best performance in terms of overall impedance properties. The cell with pristine Esp-PVAM showed higher impedance in the early activation stage, suggesting lower lithium-ion transport capability compared to the Dip 1%PVDF@Esp-PVAM cell after long-term cycling. This indicates that the cycling stability of pristine Esp-PVAM can be improved by dip coating with a hydrophilic PVDF polymer. The AC impedance results confirm that impregnating the Esp-PVAM membrane with PVDF polymer enhances the battery's long-term cycling performance. However, cells with Dip 3%PVDF@Esp-PVAM separators showed high total impedance, indicating that excessive PVDF blocks the pores of the nonwoven membrane, slowing lithium-ion transport impairing cell performance. Thus, modifying the Esp-PVAM composite separator with an optimal amount of PVDF polymer (1 wt%) enhances the long-term cycling stability of Li-ion batteries.

In addition, AC impedance analysis was further utilized to obtain the lithium-ion diffusion coefficient (D_{Li}^{+}) and exchange current density (J_0) by using Eqns. (6) and (7), as follows:

$$D_{Li+}\left(cm^2\ s^{-1}\right)=\left(\frac{2RT}{n^2\sqrt{2}^2F^2\sigma AC_{Li}}\right)^2=\frac{2R^2T^2}{n^4F^4\sigma^2A^2C_{Li}^2} \tag{6}$$

$$J_0\left(A\ cm^{-2}\right)=\frac{i_0}{A}=\frac{RT}{nFR_{ct}A} \tag{7}$$

From the Nyquist plot, the Warburg impedance in the low-frequency region is the major parameter for calculating the lithium-ion diffusion coefficient. In that region, the frequency is converted to ω (ω = 2πf; here, ω is the angular frequency, f is the frequency) to determine the linear relationship against Z' *vs.* $\omega^{-1/2}$ (Fig. 7(E) and (F)), and the average slope obtained from the linear fit is substituted into equation. (6) to calculate the D_{Li}^{+} values for the cells based on different membranes and results are summarized in Table S4. These results showed that the cell based on the Dip 1%PVDF@Esp-PVAM composite separator exhibited much greater D_{Li}^{+} and J_0 values after long-term cycling for 100 cycles at a rate of 1C/1C; these results also prove that an appropriate amount of PVDF polymer coating can effectively increase the lithium-ion diffusion coefficient. In contrast, it was also found that the impregnation of excess PVDF polymer into the Esp-PVAM composite separators had a negative impact on the cell performance due to pore blocking after long-term charge/discharge cycles. Overall, the Dip 1%PVDF@Esp-PVAM composite separators exhibited excellent physical and electrochemical properties; thus, it achieved outstanding electrochemical performance at high C-rates. As shown in Table 1, the obtained results indicate that the Dip 1%PVDF@Esp-PVAM composite separator is more comparable to previously reported LIB composite separators [24,27–29,31].

4. Conclusions

In this study, a dip coating method was used to impregnate Esp-PVAM nonwoven composite separators with 1 % or 3 % PVDF polymer to investigate its impact on battery safety and stability. This method ensured uniform polymer distribution, controlling pore size on the membrane surface. Surface morphology analysis confirmed the presence of a uniform PVDF polymer coating on the Esp-PVAM nanofibers. Consequently, the Dip 1 % PVDF@Esp-PVAM composite separator achieved higher electrolyte uptake than Dip 3 % PVDF@Esp-PVAM due to its high porosity. Electrochemical performance and thermal stability evaluations of electrospun PVAM-based composite separators showed significant improvements over commercially available PE separators. The pristine Esp-PVAM, Dip 1 % PVDF@Esp-PVAM, and Dip 3 % PVDF@Esp-PVAM composite separators exhibited higher ionic conductivity and lower activation energy, primarily due to enhanced liquid electrolyte uptake and excellent wettability. Incorporation of PVDF polymer, especially at an optimal concentration of 1 wt%, significantly enhanced the mechanical strength, thermal stability, and electrochemical performance of the separators. Thermal shrinkage tests indicated that PVDF-coated separators maintain structural integrity at elevated temperatures, outperforming PE separators. DSC and TGA analyses confirmed the improved thermal stability of the composite separators due to the PVDF coating. Electrochemical tests in half-cells showed that the PVDF-coated Esp-PVAM separators, particularly Dip 1 % PVDF@Esp-PVAM, provided better charge/discharge capacities and cycling stability. AC impedance analysis revealed lower charge

Table 1
Comparison of the properties and performance of the Dip 1%PVDF@Esp-PVAM composite separators with previously reported composite separators.

Composite Separator	Thickness (μm)	Porosity (%)	Electrolyte uptake (%)	σ_i (S cm^{-1})	Cathode	Capacity retention (CR %)	Ref.
Al_2O_3-PI	27	70.4	440.2	3.64×10^{-4}	NCM523 + $LiMn_2O_4$	95.5 % (1C, 200 cycles)	[28]
PVDF/Al_2O_3	74	55.8	152.4	2.23×10^{-3}	$LiMn_2O_4$	98.2 % (1C, 100 cycles)	[24]
ZIF-8/CNF	32	55	–	1.41×10^{-3}	$LiFePO_4$	88.2 % (0.5C, 100 cycles)	[31]
Zeolite/PAN1.5	45	68.3	308.1	2.16×10^{-3}	$LiFePO_4$	99.5 % (0.5C, 100 cycles)	[29]
PE-PVDF	26	61.4	208.0	1.53×10^{-3}	NCM111	70.0 % (0.5C, 200 cycles)	[27]
Dip 1%PVDF@Esp-PVAM	**24**	**79.0**	**550.3**	**7.75×10^{-4}**	**NCM811**	**93.4 % (1C, 100 cycles)**	**This work**

transfer resistance and total impedance, confirming superior ionic conductivity and long-term stability. Lithium-ion diffusion coefficient calculations based on Warburg impedance demonstrated enhanced ion transport properties for PVDF-coated separators. Esp-PVAM composite separators, especially those with 1 wt% PVDF coating, offer a promising alternative to conventional PE separators, providing improved mechanical strength, thermal stability, and electrochemical performance. These advancements suggest PVAM-based composite separators are well-suited for high-performance and safe LIB applications.

CRediT authorship contribution statement

Xiao-Wei Wu: Methodology, Investigation, Formal analysis, Data curation. **Manojkumar Seenivasan:** Writing – review & editing, Methodology. **Chelladurai Karuppiah:** Writing – original draft, Supervision, Methodology, Conceptualization. **Bo-Rong Zhang:** Formal analysis, Data curation. **Jeng-Ywan Shih:** Supervision, Conceptualization. **Ying-Jeng James Li:** Supervision, Methodology. **Tai-Feng Hung:** Supervision, Methodology. **Wen-Chen Chien:** Supervision, Project administration. **Sayee Kannan Ramaraj:** Supervision, Conceptualization. **Rajan Jose:** Supervision, Conceptualization. **Chun-Chen Yang:** Writing – review & editing, Supervision, Project administration, Methodology, Conceptualization.

Declaration of competing interest

The authors declare that they have no known competing financial interests or personal relationships that could have appeared to influence the work reported in this paper.

Acknowledgments

Financial support from the Ministry of Science and Technology, Taiwan (Project No: MOST 108-2221-E-131 -022-MY3) is gratefully acknowledged. The corresponding author expresses gratitude for the financial support provided by Chang Gung University (URRPD2N0021).

Appendix A. Supplementary data

Supplementary data to this article can be found online at https://doi.org/10.1016/j.heliyon.2024.e34436.

References

[1] S.C. Ma, Y. Fan, L. Feng, An evaluation of government incentives for new energy vehicles in China focusing on vehicle purchasing restrictions, Energy Pol. 110 (2017) 609–618, https://doi.org/10.1016/j.enpol.2017.07.057.
[2] J. Brady, M. O'Mahony, Travel to work in Dublin. the potential impacts of electric vehicles on climate change and urban air quality, Transport. Res. Transport Environ. 16 (2011) 188–193, https://doi.org/10.1016/j.trd.2010.09.006.
[3] Y. Miao, P. Hynan, A. Von Jouanne, A. Yokochi, Current li-ion battery technologies in electric vehicles and opportunities for advancements, Energies 12 (2019) 1–20, https://doi.org/10.3390/en12061074.
[4] P.V. Chombo, Y. Laoonual, A review of safety strategies of a Li-ion battery, J. Power Sources 478 (2020) 228649, https://doi.org/10.1016/j.jpowsour.2020.228649.
[5] S. Zhong, B. Yuan, Z. Guang, D. Chen, Q. Li, L. Dong, Y. Ji, Y. Dong, J. Han, W. He, Recent progress in thin separators for upgraded lithium ion batteries, Energy Storage Mater. 41 (2021) 805–841, https://doi.org/10.1016/j.ensm.2021.07.028.
[6] Y. Li, Q. Li, Z. Tan, A review of electrospun nanofiber-based separators for rechargeable lithium-ion batteries, J. Power Sources 443 (2019) 227262, https://doi.org/10.1016/j.jpowsour.2019.227262.
[7] V. Deimede, C. Elmasides, Separators for lithium-ion batteries: a review on the Production Processes and recent Developments, Energy Technol. 3 (2015) 453–468, https://doi.org/10.1002/ente.201402215.
[8] L. Liu, J. Xu, S. Wang, F. Wu, H. Li, L. Chen, Practical evaluation of energy densities for sulfide solid-state batteries, eTransportation 1 (2019) 100010, https://doi.org/10.1016/j.etran.2019.100010.
[9] W. Jiang, Y. Han, Y. Ding, Sepiolite and ZIF-67 co-modified PAN/PVdF-HFP nanofiber separators for advanced Li-ion batteries, Nanotechnology 33 (2022) 425601, https://doi.org/10.1088/1361-6528/ac8061.
[10] S. Zhang, J. Luo, M. Du, F. Zhang, X. He, Highly porous zeolitic imidazolate framework-8@bacterial cellulose composite separator with enhanced electrolyte absorption capability for lithium-ion batteries, Cellulose 29 (2022) 5163–5176, https://doi.org/10.1007/s10570-022-04598-3.
[11] S.H. Senthilkumar, B. Ramasubramanian, R.P. Rao, V. Chellappan, S. Ramakrishna, Advances in electrospun materials and methods for Li-ion batteries, Polymers 15 (2023), https://doi.org/10.3390/polym15071622.
[12] S.N. Banitaba, A. Ehrmann, Application of electrospun nanofibers for fabrication of versatile and highly efficient electrochemical devices: a review, Polymers 13 (2021), https://doi.org/10.3390/polym13111741.
[13] Y. Zhai, X. Wang, Y. Chen, X. Sang, H. Liu, J. Sheng, Y. Wu, X. Wang, L. Li, Multiscale-structured polyvinylidene fluoride/polyacrylonitrile/vermiculite nanosheets fibrous membrane with uniform Li+ flux distribution for lithium metal battery, J. Membr. Sci. 621 (2021) 118996, https://doi.org/10.1016/j.memsci.2020.118996.
[14] P.J. Kim, Surface-functionalized separator for stable and reliable lithium metal batteries: a review, Nanomaterials 11 (2021), https://doi.org/10.3390/nano11092275.
[15] Y. Lee, M.H. Ryou, M. Seo, J.W. Choi, Y.M. Lee, Effect of polydopamine surface coating on polyethylene separators as a function of their porosity for high-power Li-ion batteries, Electrochim. Acta 113 (2013) 433–438, https://doi.org/10.1016/j.electacta.2013.09.104.
[16] Z. Jahan, M.B.K. Niazi, Ø.W. Gregersen, Mechanical, thermal and swelling properties of cellulose nanocrystals/PVA nanocomposites membranes, J. Ind. Eng. Chem. 57 (2018) 113–124, https://doi.org/10.1016/j.jiec.2017.08.014.
[17] J. Yan, Y. Zhao, X. Wang, S. Xia, Y. Zhang, Y. Han, J. Yu, B. Ding, Polymer Template Synthesis of Soft, Light, and Robust Oxide ceramic films, iScience 15 (2019) 185–195, https://doi.org/10.1016/j.isci.2019.04.028.

[18] J. Yan, X.-K. Ma, M.-Y. Wang, J.-P. Ni, K.-Z. Gao, Y. Zhang, L.-Z. Wang, Synergistic effect of dispersant and wetting reagent on wettability, thermal Stability and electrochemical properties of PVDF-coating polyethylene separator for lithium-ion batteries, Int J Electrochem Sc 16 (2021) 210747, https://doi.org/10.20964/2021.07.49.
[19] M. Cai, D. Yuan, X. Zhang, Y. Pu, X. Liu, H. He, L. Zhang, X. Ning, Lithium ion battery separator with improved performance via side-by-side bicomponent electrospinning of PVDF-HFP/PI followed by 3D thermal crosslinking, J. Power Sources 461 (2020) 1–10, https://doi.org/10.1016/j.jpowsour.2020.228123.
[20] W. Liu, J. Chen, Z. Chen, K. Liu, G. Zhou, Y. Sun, M.S. Song, Z. Bao, Y. Cui, Stretchable lithium-ion batteries enabled by device-Scaled Wavy structure and Elastic-Sticky separator, Adv. Energy Mater. 7 (2017) 1–6, https://doi.org/10.1002/aenm.201701076.
[21] S. Wu, J. Ning, F. Jiang, J. Shi, F. Huang, Ceramic Nanoparticle-Decorated melt-electrospun PVDF nanofiber membrane with enhanced performance as a lithium-ion battery separator, ACS Omega 4 (2019) 16309–16317, https://doi.org/10.1021/acsomega.9b01541.
[22] C. Karuppiah, Y.C. Hsieh, S.L. Beshahwured, X.W. Wu, S.H. Wu, R. Jose, S.J. Lue, C.C. Yang, Poly(vinyl alcohol)/melamine composite containing LATP nanocrystals as a high-Performing nanofibrous membrane separator for high-power, high-voltage lithium-ion batteries, ACS Appl. Energy Mater. 3 (2020) 8487–8499, https://doi.org/10.1021/acsaem.0c01132.
[23] M.I. Peñas, C. Ocando, E. Penott-Chang, M. Safari, T.A. Ezquerra, E. Rebollar, A. Nogales, R. Hernández, A.J. Müller, Nanostructural organization of thin films prepared by sequential dip-coating deposition of poly(butylene succinate), poly(ε-caprolactone) and their copolyesters (PBS-ran-PCL), Polymer 226 (2021), https://doi.org/10.1016/j.polymer.2021.123812.
[24] D. Wu, L. Deng, Y. Sun, K.S. Teh, C. Shi, Q. Tan, J. Zhao, D. Sun, L. Lin, A high-safety PVDF/Al2O3 composite separator for Li-ion batteries via tip-induced electrospinning and dip-coating, RSC Adv. 7 (2017) 24410–24416, https://doi.org/10.1039/c7ra02681a.
[25] K. Jantanasakulwong, N. Homsaard, P. Phengchan, P. Rachtanapun, N. Leksawasdi, Y. Phimolsiripol, C. Techapun, P. Jantrawut, Effect of dip coating polymer solutions on properties of thermoplastic cassava starch, Polymers 11 (2019), https://doi.org/10.3390/polym11111746.
[26] P.T.P. Aryanti, G. Trilaksono, A. Hotmaida, M.A. Afifah, F.P. Pratiwi, N. Udini, F.A. Nugroho, Preparation of polypropylene/PVDF composite membrane by dip-coating method, IOP Conf. Ser. Mater. Sci. Eng. 1115 (2021) 012028, https://doi.org/10.1088/1757-899x/1115/1/012028.
[27] Y. Wang, C. Yin, Z. Song, Q. Wang, Y. Lan, J. Luo, L. Bo, Z. Yue, F. Sun, X. Li, Application of PVDF organic particles coating on polyethylene separator for lithium ion batteries, Materials 12 (2019), https://doi.org/10.3390/ma12193125.
[28] J. Lee, C.L. Lee, K. Park, I.D. Kim, Synthesis of an Al2O3-coated polyimide nanofiber mat and its electrochemical characteristics as a separator for lithium ion batteries, J. Power Sources 248 (2014) 1211–1217, https://doi.org/10.1016/j.jpowsour.2013.10.056.
[29] D. Chen, X. Wang, J. Liang, Z. Zhang, W. Chen, A novel electrospinning polyacrylonitrile separator with dip-coating of zeolite and phenoxy resin for Li-ion batteries, Membranes 11 (2021), https://doi.org/10.3390/membranes11040267.
[30] T. Remiš, P. Bělský, S.M. Andersen, M. Tomáš, J. Kadlec, T. Kovářík, Preparation and Characterization of poly(vinyl alcohol) (PVA)/SiO2, PVA/Sulfosuccinic Acid (SSA) and PVA/SiO2/SSA membranes: a Comparative study, J. Macromol. Sci., Part B: Phys. 59 (2020) 157–181, https://doi.org/10.1080/00222348.2019.1697023.
[31] X. Sun, M. Li, S. Ren, T. Lei, S.Y. Lee, S. Lee, Q. Wu, Zeolitic imidazolate framework-cellulose nanofiber hybrid membrane as Li-Ion battery separator: Basic membrane property and battery performance, J. Power Sources 454 (2020), https://doi.org/10.1016/j.jpowsour.2020.227878.